ATMOSPHERIC AND OCEANIC SCIENCE LETTERS, 2013, VOL. 6, NO. 5, 273–278

Projected Changes of Palmer Drought Severity Index under an RCP8.5 Scenario

ZHOU Tian-Jun[1,2] and HONG Tao[1,3]

[1] *State Key Laboratory of Numerical Modeling for Atmospheric Sciences and Geophysical Fluid Dynamics, Institute of Atmospheric Physics, Chinese Academy of Sciences, Beijing 100029, China*
[2] *Climate Change Research Center, Chinese Academy of Sciences, Beijing 100029, China*
[3] *University of Chinese Academy of Sciences, Beijing 100049, China*

Received 25 March 2013; revised 22 April 2013; accepted 22 April 2013; published 16 September 2013

Abstract The potential change of drought measured by the Palmer Drought Severity Index (PDSI) is projected by using a coupled climate system model under a Representative Pathway 8.5 (RCP8.5) scenario. The PDSI changes calculated by two potential evapotranspiration algorithms are compared. The algorithm of Thornthwaite equation overestimates the impact of surface temperature on evaporation and leads to an unrealistic increasing of drought frequency. The PM algorithm based on the Penman-Monteith equation is physically reasonably and necessary for climate change projections. The Flexible Global Ocean-Atmosphere-Land System model, Spectral Version 2 (FGOALS-s2) projects an increasing trend of drought during 2051–2100 in tropical and subtropical areas of North and South America, North Africa, South Europe, Southeast Asia, and the Australian continent. Both the moderate drought (PDSI < –2) and extreme drought (PDSI < –4) areas show statistically significant increasing trends under an RCP8.5 scenario. The uncertainty in the model projection is also discussed.

Keywords: palmer drought severity index, projection, RCP8.5 scenario, climate model

Citation: Zhou, T.-J., and T. Hong, 2013: Projected changes of palmer drought severity index under an RCP8.5 scenario, *Atmos. Oceanic Sci. Lett.*, **6**, 273–278, doi:10.3878/j.issn.1674-2834.13.0032.

1 Introduction

Drought is a recurring extreme climate event over land characterized by below-normal precipitation over a period of several months to several years, or even a few decades. It is one of the world's most destructive natural hazards, and causes more deaths and displacement than cyclones, floods and earthquakes combined. Since the 1970s, the land area affected by drought has increased substantially due to recent drying trends over Africa, southern Europe, East and South Asia, and eastern Australia (Dai, 2011a). Projecting how the drought would change in the future is of crucial importance to help countries to move from drought crisis management to drought disaster risk reduction.

Many drought indices have been developed to quantify drought. The Palmer Drought Severity Index (PDSI), which was originally developed by Palmer (1965) with the intent to measure the cumulative departure in surface water balance, is one of the most prominent indices of meteorological drought (Dai, 2011b). The PDSI index has been widely used in Chinese aridity studies. For example, the PDSI was calculated by using station data of monthly air temperature and precipitation in China during the period 1951–2003. Significant increases of drought areas are found in North China (Hua et al., 2011; Zou et al., 2005). The drought changes are later demonstrated by analysis on the monsoon circulation changes (Yu et al., 2004; Yu and Zhou, 2007; Zhou et al., 2009). The interannual variability of PDSI over China associated with ENSO activities during 1951–2000 was discussed by Su and Wang (2007), significant correlations are found in the periods of 1951–1962 and 1976–1991. But during the periods of 1963–1975 and 1992–2000, the link of PDSI changes over China to ENSO is weak. Moisture variability across China and Mongolia during 1951–2005 was investigated using the monthly PDSI dataset released by Dai et al. (2004). Based on rotated Empirical Orthogonal Function (REOF) results, it is proposed that China and Mongolia should be divided into ten coherent moisture divisions. Moisture variations within each division are generally coherent, but may show either similar or contrasting co-variability with adjacent divisions (Li et al., 2009). All these studies demonstrated that the PDSI index is a useful measure for quantify the wetness and dryness changes over China.

The frequency, intensity, and duration of droughts are expected to rise in several parts of the world as a result of climate change, but quantitative projections depend on climate models. The main motivation of the current study is to examine the potential change of PDSI index under Representative Concentration Pathway 8.5 (RCP8.5) (Moss et al., 2010) by using the output of Institute of Atmospheric Physics (IAP)/State Key Laboratory of Numerical Modeling for Atmospheric Sciences and Geophysical Fluid Dynamics (LASG) climate system model Flexible Global Ocean-Atmosphere-Land System (FGOALS).

2 Model and experiment description

The climate system model used in this study is the FGOALS developed at IAP/LASG. The model version we

Corresponding author: ZHOU Tian-Jun, zhoutj@lasg.iap.ac.cn

used is FGOALS-s2, which employs the National Center for Atmospheric Research (NCAR) flux coupler version 6 (CPL6), the Spectral Atmospheric Model of IAP/LASG version 2 (SAMIL2), LASG/IAP climate ocean model version 2 (LICOM2), the Community Land Model version 3 (CLM3), and Community Sea Ice Model version 5 (CSIM5). The atmospheric component SAMIL2 holds a horizontal resolution of about 2.81° longitude × 1.66° latitude and 26 levels in the vertical. The horizontal resolution of ocean component LICOM2 is about 1° longitude × 1° latitude in extra-tropical zone and 0.5° longitude × 0.5° latitude in tropics and there are 30 vertical levels. For details of the coupled models, the reader is referred to Bao et al. (2013).

The Representative Concentration Pathways scenarios include time paths for concentrations of the full suite of greenhouse gases (GHGs) and aerosols and chemically active gases, as well as land use/land cover changes. RCP8.5 is the high pathway for which radiative forcing reaches > 8.5 W m^{-2} by 2100 and continues to rise over time (Moss et al., 2010). In our RCP8.5 scenario projection with FGOALS-s2 model, the land use/land cover changes were not specified.

Detailed descriptions of how the PDSI is computed can be found in Palmer (1965) and Alley (1984). The potential evapotranspiration (PE) can be estimated by two algorithms. The first, developed by Thornthwaite (1948), is based on the knowledge of the temperature and latitude, and hereinafter will be designated PE_th. The second, developed by Burke et al. (2006) and designated PE_pm, employs a more sophisticated Penman-Monteith equation to account for the effects of surface temperature, surface specific humidity, wind speed, surface air pressure, and surface net solar radiation. The PDSI calculated by using the algorithms is designated PDSI_th or PDSI_pm in the following analysis. We compared the results calculated by these two algorithms, using codes for calculating the indices provided by Dr. Aiguo DAI (Dai, 2011a, b).

3 Results

We focus on the future changes of PDSI index in our analysis. Based on recommendations of the Intergovernmental Panel on Climate Change (IPCC) Fifth Assessment Report (AR5), the anomalies were calculated relative to a reference period of 1986–2005. The 1986–2005 climatology is derived from the historical climate simulation of FGOALS-s2. The 1986–2005 climatology of surface air temperature in the historical climate simulation of FGOALS-s2 is warmer than observed (Zhou et al., 2013), and the anomalies in the projections are calculated relative to the model climatology rather than that of the observation. The observed changes of drought in the last few decades are dominated by Pacific Decadal Oscillation (PDO) (Ma and Shao, 2006; Ma, 2007). Since the PDO is an internal variability mode of the climate system, the specified external forcings in the historical climate simulation are unable to reproduce the observed PDO phase transitions; the consistency between the simulated and observed PDO phases are generally poor.

The projected changes of global average annual mean surface air temperature, precipitation, and PDSI are shown in Fig. 1. The average was derived only over the land area from 58.75°S to 76.25°N. Following the increase of greenhouse gases (GHGs), the model projection exhibits increasing trends in both the surface air temperature and precipitation. The linear trend estimated as the slope of a straight line fitted in a least squares sense to the simulated time series is 3.2 K per 100 years for temperature and 0.15 mm d^{-1} per 100 years for precipitation. Both two trends are statistically significant at the 0.01 level. The increasing trend of global land precipitation follows the constraint of water vapor according to the Clausius- Clapeyron equation (Held and Soden, 2006). Note that the warming trend is overestimated by the FGOALS-s2 model due to its high climate sensitivity to GHGs (Chen et al., 2013).

Following the increases of surface temperature and precipitation, the global average PDSI over the land calculated by using PE_th and PE_pm algorithms shows different trends in the 21st century (Fig. 1c). The former exhibits a decreasing trend of –0.76 per 100 years, while the latter shows an increasing trend of 0.65 per 100 years, both are statistically significant at the 0.01 level. Thus the PDSI trends derived from two algorithms for PE calculation show contrasting results: under the same high pathway of RCP8.5, the future world would witness a drying

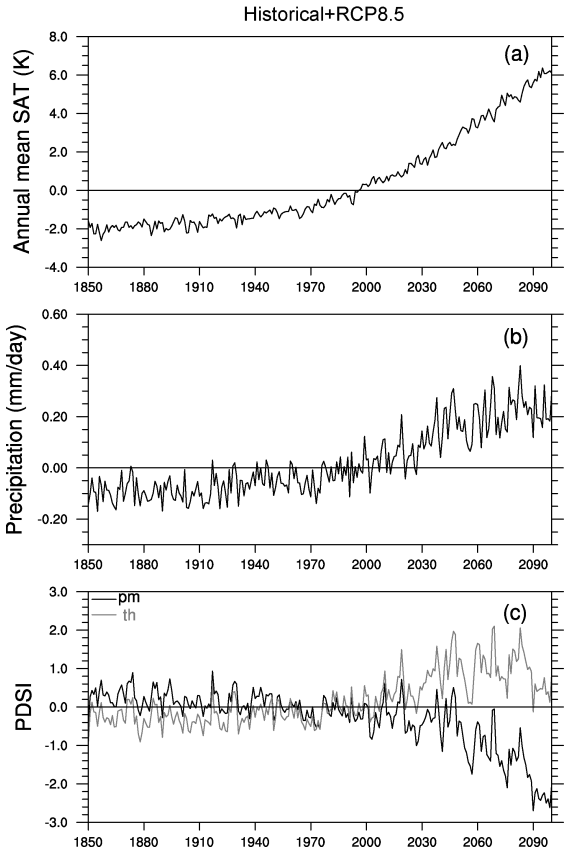

Figure 1 (a) The annual mean surface air temperature SAT, (b) precipitation, and (c) PDSI_pm and PDSI_th values averaged over global land domain derived from the historical simulation and RCP8.5 projection of FGOALS-s2 model.

land with the PE_th algorithm, but a wetting land with the PE_pm algorithm. A further analysis of the changes of global average of net precipitation (viz. precipitation minus evaporation) reveals that the PE_th overestimates the impact of temperature on evaporation, the increase of evaporation overwhelms the increase of precipitation, and we observe a decreasing trend of PDSI_th (figures not shown).

The soil moisture is a good index for representing drought and a reasonable calculation of PDSI distribution should be consistent with the pattern of soil moisture. In Fig. 2, twenty-year average changes of the PDSI derived from the two algorithms are compared to the soil moisture for a long-term (2081–2100) mean relative to a reference period of 1986–2005. The pattern of PDSI_pm is different to PDSI_th in North and South Africa, East Australia, and South America (Figs. 2a–b). In particular, the PDSI_th shows a drying trend in South Africa and South America (Fig. 2a), but the PDSI_pm exhibits a wetter trend. It should be noted that the pattern of PDSI_pm is generally consistent with that of soil moisture (Fig. 2c). Thus, the PDSI_pm is physically more reasonable. The PDSI_th overestimates the increase of drought frequency in most areas in particular the South Africa and South America, as evidenced in Fig. 2d.

Why does the PM_th algorithm reproduce a PDSI pattern that is physically inconsistent with that of soil moisture? Both surface temperature (through potential evapotranspiration) and precipitation changes contribute to the final change of PDSI. To estimate the direct impact of global warming on the PDSI trends, we computed the PDSI with all forcing except temperature changes, i.e., monthly temperature climatology was used for this dT=0 case. We also estimate the direct impact of precipitation on the PDSI trends by computing the PDSI with all forcing except precipitation changes, i.e., monthly precipitation climatology was used for this dP=0 case. Note that in the real world, changes in precipitation are coupled to temperature changes. Both the dT=0 and dP=0 cases are used here only to estimate the direct impact of temperature/precipitation on PDSI as Dai (2011b).

The 2051–2100 trend patterns between the all forcing and the dT=0/dP=0 case are compared in Fig. 3. Without the surface warming, most of the drying regions seen in the all forcing case (Fig. 3a) disappear in the dT=0 case (Fig. 3b), except for North Africa, southern China, Australia, and tropical parts of North and South America, where the drying trends to a large extent result from precipitation decrease. Without the effect of surface warming, most extra-tropical regions of the Eurasian continent, North and South American continent, and South Africa would become wetter (Fig. 3b). Thus, the regional scale PDSI drying trends in these areas result from the warming trends rather than precipitation changes. This is further confirmed in Fig. 3c. Without precipitation changes, the global land areas all would become drier due to enhanced evaporation associated with global warming (Fig. 3c). Thus our analysis demonstrates that the PDSI derived from PM_th algorithm is dominated by the surface temperature in most areas. The PM_th overestimates the impact of temperature on evaporation and results in an unrealistic increase in drought frequency, especially in South Africa. The overestimation of drought by PDSI_th relative to PDSI_pm is more evident in Fig. 3d. Note in East Asia south to 30°N, both the decrease of precipitation and the increase of surface warming are responsible for the drying trend. Similar situations are seen in North Africa, Australia, and tropical parts of North and South America.

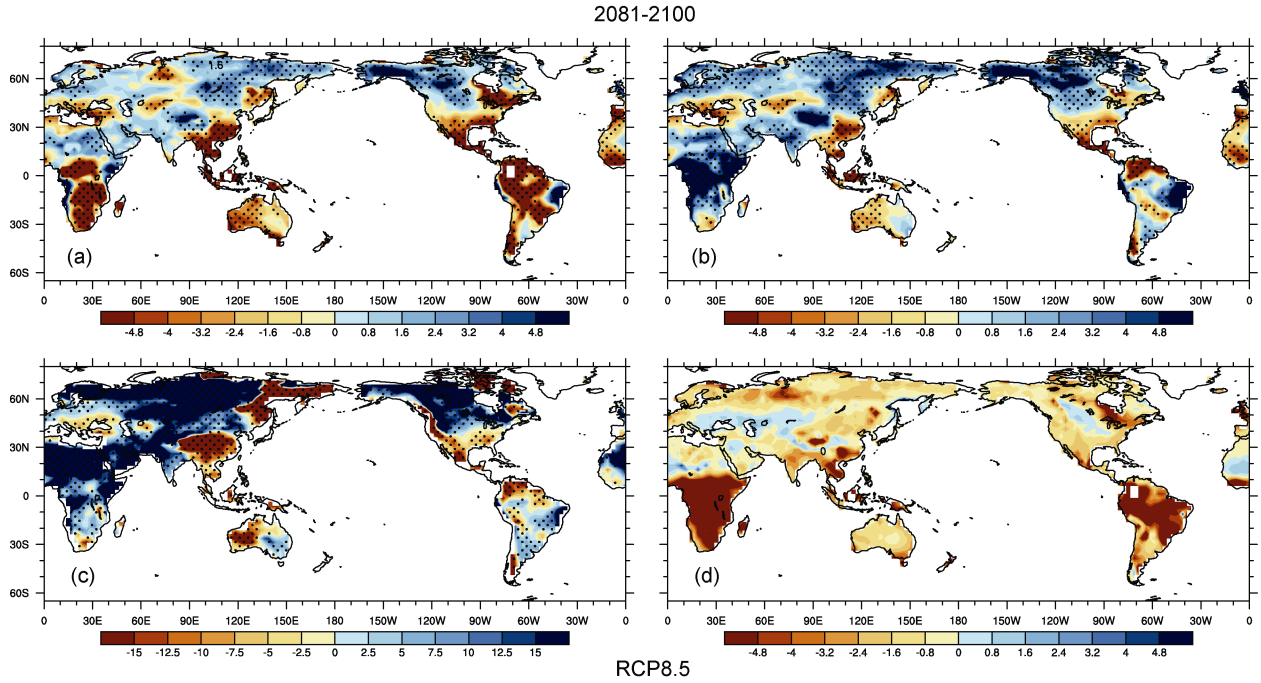

Figure 2 Maps of (a) PDSI_th, (b) PDSI_pm, and (c) soil moisture changes in 2081–2100 with respect to 1986–2005 in the RCP8.5 scenario projected by FGOALS-s2. The difference between PDSI_th and PDSI_pm is shown in (d). Black dots denote areas where the 20-year mean differences are statistically at the 95% confidence level based on Student's *t*-test.

We further compare the contribution of surface temperature and precipitation to PDSI trend derived from PM_pm algorithm in Figs. 4a–c. The PDSI trend is also compared to the trend of soil moisture in Fig. 4d. It is evident that the pattern of PDSI_pm is nearly identical to that of soil moisture, indicating that the PDSI derived from the PM_pm algorithm is physically reasonable. Both the surface temperature and precipitation changes are in favor of a drier (wetter) condition in North (South) Africa. The drier East Asia south to 30°N is dominated by the precipitation changes, although the contribution of surface temperature is also evident. Note that the soil moisture trend in North Africa is not consistent with that of PDSI_pm and the reason deserves further study.

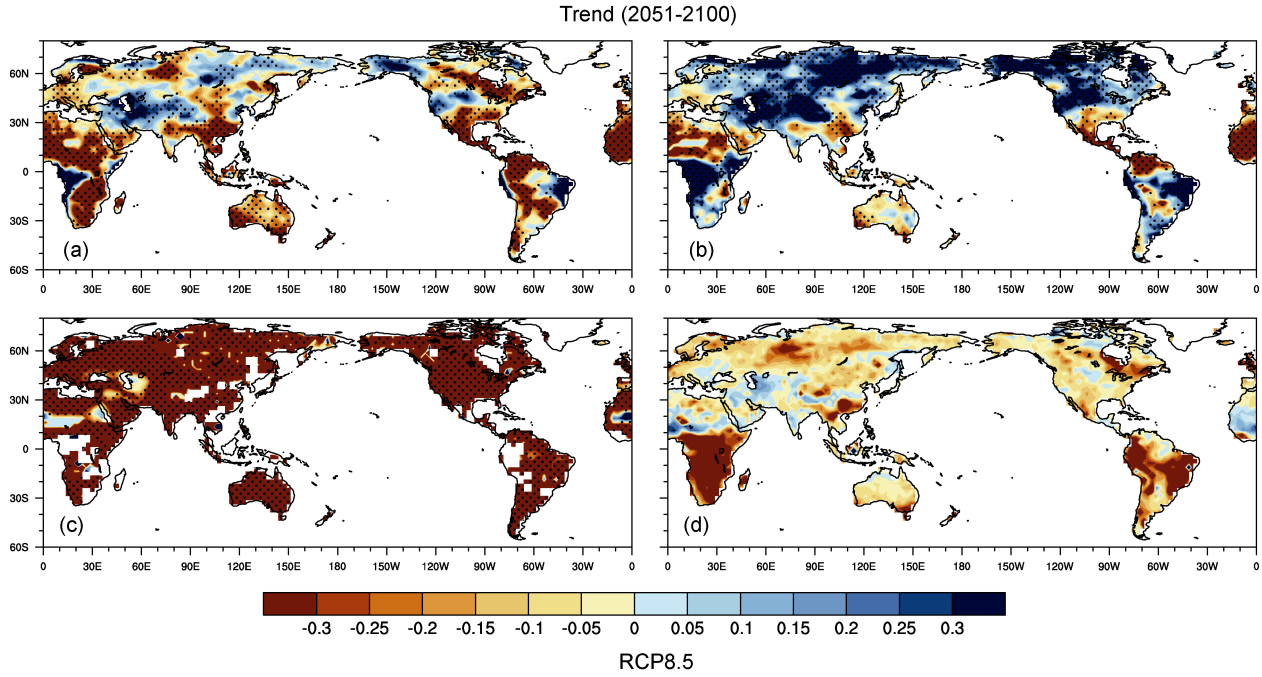

Figure 3 Trend maps (brown, drying, units: change per 50 years) of the annual PDSI_th from 2051–2100 computed using (a) all forcing data, (b) all but no temperature changes, and (c) all but no precipitation changes. The difference between PDSI_th and PDSI_pm is shown in (d). Black dots denote areas where the trends are statistically at the 95% confidence level.

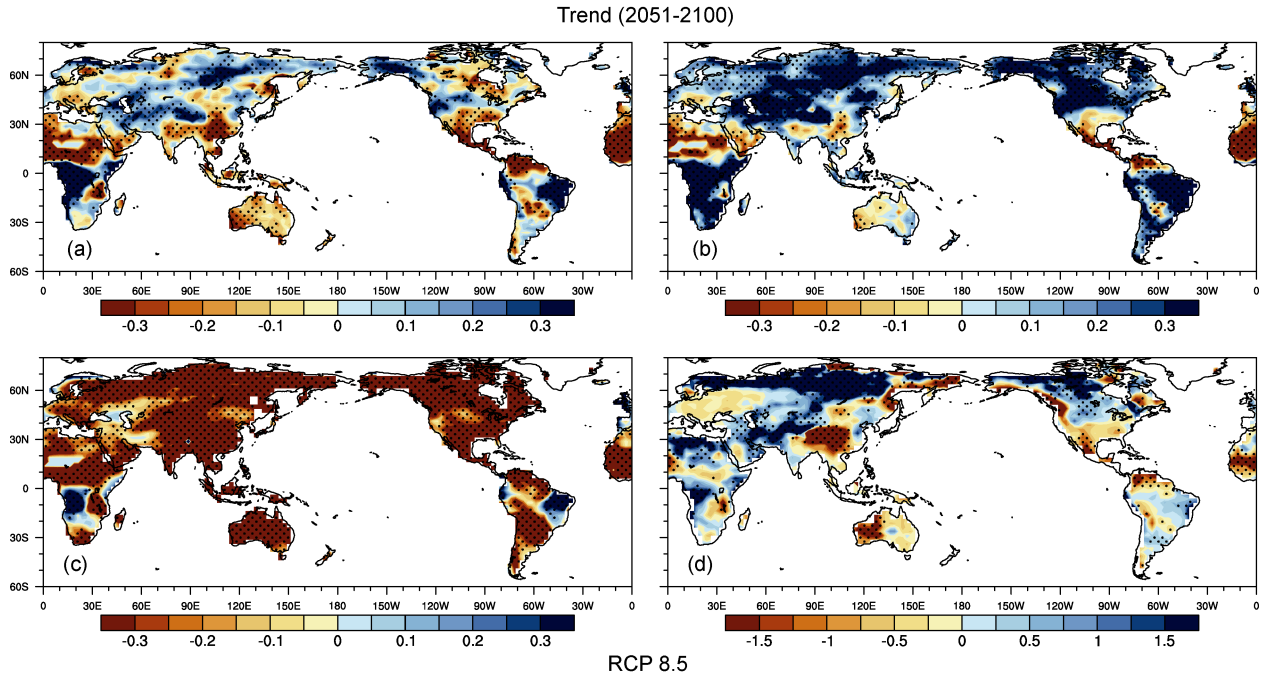

Figure 4 Trend maps (brown, drying, units: change per 50 years) of the annual PDSI_pm from 2051–2100 computed using (a) all forcing data, (b) all but no temperature changes, and (c) all but no precipitation changes. The corresponding trend of soil moisture is shown in (d) (Units: kg m^{-2} per 50 years). Black dots denote areas where the trends are statistically at the 95% confidence level.

The PDSI change projected by 22 Coupled Model Intercomparison Project 3 (CMIP3) climate models under a SRES A1B scenario (Dai, 2011a) exhibits an increasing trend of drought in tropical and subtropical areas of North and South America, North and South Africa, South Europe, Southeast Asia, and the Australian continent. The results of PSDI_pm shown here are different to CMIP3 models in South Africa and South Europe. The projected increasing trend of drought in North and South America are weaker than that of CMIP3 model.

We further illustrate the impacts of global warming and precipitation on the PDSI changes in Figs. 5a–b. It is evident that the changes of precipitation would lead to a wetting trend while the changes of surface temperature would lead to drying trend in PDSI_pm, but the changes of PDSI_pm cannot be solely accounted by precipitation and temperature changes (Fig. 5a). The PDSI_th drying trend is mainly the result of the surface temperature changes in the context of a global average. Without the changes of surface temperature, the changes of precipitation would lead to a wetter rather than drier condition (Fig. 5b). The PM_th algorithm overestimates the evaporation change due to surface temperature and leads to a drier future.

What can be said about future changes of drought in different categories? We examine the changes of moderate drought (PDSI < –2) and extreme drought (PDSI< –4) areas in Figs. 5c–d. Both the moderate drought and extreme drought exhibit enhanced trends in 2009–2100, indicating an expansion in coverage (Fig. 5c). The trends estimated as the slope of a straight line fitted in a least squares sense to the time series of PDSI_th (PDSI_pm) are 28% per 100 years (16% per 100 years) for moderate drought, and 25% per 100 years (11% per 100 years) for extreme drought, respectively. Both are statistically at the 1% confidence level. The trends derived from PDSI_pm are weaker than that of PDSI_th.

Following the global warming trend, both the moderate wet (PDSI > 2) and extreme wet (PDSI > 4) areas show a weak increasing trends (Fig. 5d). The trend for PDSI_pm (PDSI_th) is 18% per 100 years (6% per 100 years) for the moderate wet area. The corresponding trends for the extreme wet area are 12% per 100 years (4% per 100 years) for PDSI_pm (PDSI_th). The PDSI_pm and PDSI_th are qualitatively consistent in measuring the trends of moderate and extreme drought/wet area changes.

4 Summary and concluding remarks

The potential change of drought under a RCP8.5 scenario is projected by using a coupled climate system model. The PDSI is used to quantify the drought. The PDSI changes calculated by two PM algorithms are compared. The results show that the global average of land precipitation would increase due to the increases of lower tropospheric water vapor according to the Clausius-Clapeyron equation. The potential evapotranspiration calculated by the Thornthwaite (1948) algorithms overestimates the impact of surface temperature on evaporation and leads to an unrealistic increase of drought frequency. The PDSI change calculated by using the potential evapotranspiration based on the Penman-Monteith equation is generally consistent with the change of soil moisture, and physically reasonably. The use of potential evapotranspiration calculated by Penman-Monteith equation instead of Thornthwaite (1948) algorithms is thus necessary for the climate change projection. The FGOALS-s2 model projects an increasing trend of drought during 2051–2100 in tropical and subtropical areas of North and South

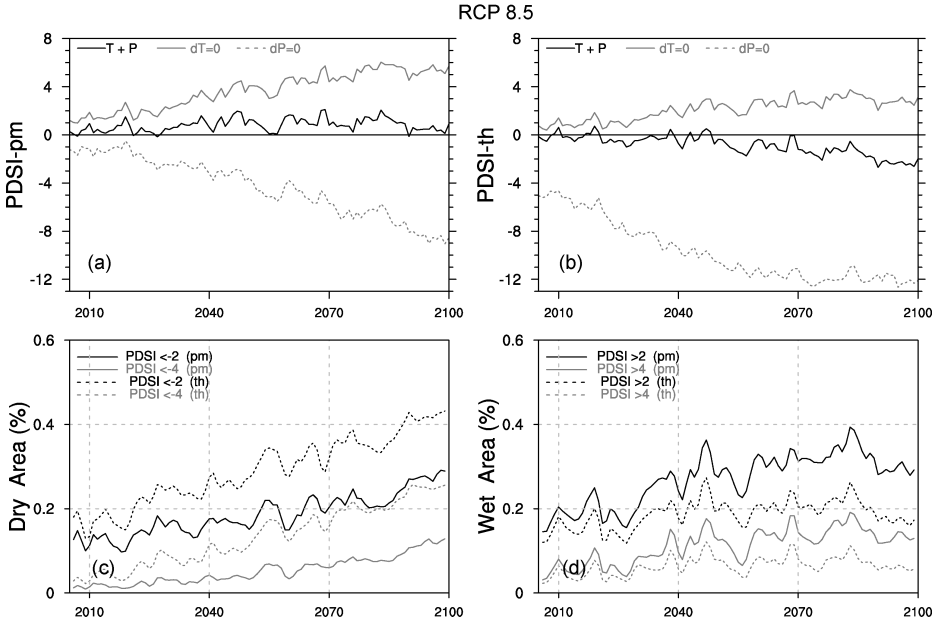

Figure 5 Time series of global land area averaged annual anomalies of (a) PDSI_pm and (b) PDSI_th using all forcing (black line), without temperature changes (grey solid line), and without precipitation changes (grey dash line); (c) global land area covered by moderate drought (PDSI< –2, black line) and extreme drought (PDSI < –4, grey line); (d) global land area covered by moderate wetness (PDSI > 2, black line) and extreme wetness (PDSI > 4, grey line).

America, North Africa, South Europe, Southeast Asia, and the Australian continent. Both the moderate drought (PDSI < –2) and extreme drought (PDSI < –4) areas show statistically significant increasing trends under RCP8.5 scenario and the PDSI_pm and PDSI_th are qualitatively consistent in measuring this trend.

Limitations of the current study should be acknowledged. The RCP8.5 scenario is a high pathway for which radiative forcing reaches > 8.5 W m^{-2} by 2100. The associated amplitude of global warming represents a high scenario. The high sensitivity of FGOALS-s2 model to GHGs (Chen et al., 2013) may also amplify the model response. Quantitative interpretation of the PDSI change patterns also requires caution, because the 1986–2005 climatology in the model world is not exactly the same as the observations. The difference of FGOALS-s2 model to CMIP3 models in the projection of regional PDSI changes such as South Africa should be addressed in the future. Multi-models inter-comparisons are needed in future studies. In addition, the soil moisture trend during 2051–2100 in North Africa shows a wetting trend, but the PDSI_pm exhibits a drying trend. Further studies are needed to understand this paradox.

Finally, to avoid the abuse of climate projection information, we acknowledge that the projections of future climate change are conditional on assumptions of climate forcing, such as different RCPs. The results are also affected by shortcomings of climate models and are inevitably subject to internal variability of the complex coupled climate system. Therefore, both the time series and the spatial patterns of PDSI changes are not "forecasts" and should not be interpreted as such.

Acknowledgements. This work is supported by the Strategic Priority Research Program-Climate Change: Carbon Budget and Related Issues of the Chinese Academy of Sciences (Grant No. XDA 05110301) and Public Science and Technology Research Funds Projects of Ocean (201105019-3). We thank Dr. Aiguo DAI of NCAR for providing the code used in calculating the PDSI values.

References

Alley, W. M., 1984: The palmer drought severity index: Limitations and assumptions, *J. Climate Appl. Meteor.*, **23**, 1100–1109.

Bao, Q., P. Lin, T. Zhou, et al., 2013: The flexible global ocean-atmosphere-land system model version: FGOALS-s2, *Adv. Atmos. Sci*., **30**, doi:10.1007/s00376-012-2113-9.

Burke, E. J., J. B. Simon, and N. Christidis, 2006: Modeling the recent evolution of global drought and projections for the twenty-first century with the Hadley centre climate model, *J. Hydrometeorol.*, **7**, 1113–1125.

Chen, X., T. Zhou, and Z. Guo, 2013: Climate sensitivities of two versions of FGOALS model to idealized radiative forcing, *Sci. China Ser. D-Earth Sci.*, in press.

Dai, A., 2011a: Drought under global warming: A review, in: *Wiley Interdisciplinary Reviews: Climate Change*, **2**, 45–65.

Dai, A., 2011b: Characteristics and trends in various forms of the palmer drought severity index during 1900–2008, *J. Geophys. Res.*, **116**, D12115, doi:10.1029/2010JD015541.

Dai, A., K. E. Trenberth, T. Qian, 2004: A global dataset of palmer drought severity index for 1870–2002: Relationship with soil moisture and effects of surface warming, *J. Hydrometeorol.*, **5**, 1117–1130.

Held, I. M., and B. J. Soden, 2006: Robust responses of the hydrological cycle to global warming, *J. Climate*, **19**, 5686–5699.

Hua, L. J., Z. G., Ma, and L. H. Zhong, 2011: A comparative analysis of primary and extreme characteristics of dry or wet status between Asia and North America, *Adv. Atmos. Sci.*, **28**(2), 352–362.

Li, J., E. R. Cook, R. D'arrigo, et al., 2009: Moisture variability across China and Mongolia: 1951–2005, *Climate Dyn.*, **32**, 1173–1186.

Ma, Z., 2007: The interdecadal dry/wet trend and shift of North China and their relationship to the Pacific Decadal Oscillation (PDO), *Chinese Sci. Bull.*, **52**(15), 2130–2139.

Ma, Z., and L. Shao, 2006: Relationship between dry/wet variation and the Pacific Decadal Oscillation (PDO) in northern China during the last 100 years, *Chinese J. Atmos. Sci.* (in Chinese), **30**, 464–474.

Moss, R. H., J. A. Edmonds, K. A. Hibbard, et al., 2010: The next generation of scenarios for climate change research and assessment, *Nature*, **46**, 747–756.

Palmer, W. C., 1965: *Meteorological Drought*, Research Paper No. 45, U. S. Department of Commerce, Washington D. C., 58pp, available at http://www.ncdc.noaa.gov/oa/climate/research/drought/palmer.pdf.

Su, M. F., and H. J. Wang, 2007: Relationship and its instability of ENSO—Chinese variations in droughts and wet spells, *Sci. China Ser. D-Earth Sci.*, **50**(1), 145–152.

Thornthwaite, C. W., 1948: An approach toward a rational classification of climate, *Geogr. Rev.*, **38**, 55–94.

Yu, R., B. Wang, and T. Zhou, 2004: Tropospheric cooling and summer monsoon weakening trend over East Asia, *Geophys. Res. Lett.*, **31**, L22212, doi:10.1029/2004GL021270.

Yu, R., and T. Zhou, 2007: Seasonality and three-dimensional structure of the interdecadal change in East Asian monsoon, *J. Climate*, **20**, 5344–5355.

Zhou, T., D. Gong, J. Li, et al., 2009: Detecting and understanding the multi-decadal variability of the East Asian summer monsoon: Recent progress and state of affairs, *Meteor. Z.*, **18**, 455–467.

Zhou, T., F. Song, and X. Chen, 2013: Historical evolutions of global and regional surface air temperature simulated by FGOALS-s2 and FGOALS-g2: How reliable are the model results? *Adv. Atmos. Sci.*, **30**, doi:10.1007/s00376-013-2205-1.

Zou, X., P. Zhai, and Q. Zhang, 2005: Variations in droughts over China: 1951–2003, *Geophys. Res. Lett.*, **32**, L04707, doi:10.1029/2004GL021853.